Chapter 9
Solar Racer—Concept Generation and Selection

9.1 Introduction

In this book, "conceptual design" describes the second stage of the design process in which a vehicle's physical envelope, its boundary, is defined. Our goals are to:

1. Select the car's shape
2. Set its major dimensions
3. Estimate the gross mass and the location of the center of gravity (CG)
4. Specify the main requirements for the drive
5. Set the main features of the driver–car interface
6. Set the main requirements for the electrical power subsystem
7. Set the number of wheels
8. Examine the stability

The design selected for continued development will satisfy, or will at least be judged to have the potential to satisfy, all of the required and more of the wished-for characteristics in Chap. 8 than its competitors.

9.2 Concept Sketch

The requirements that the solar racer must meet, in the designer's judgment, to win a cross-country solar car race have been written in the specification. Now, take a blank sheet of crosshatched paper, set the scale of the smallest square, and begin to design to meet these requirements. First, lay out the specified bounding dimensions; this gives the box in which the car must fit. Then, make a to-scale, freehand concept sketch in three views that fits within the bounding box and incorporates the main features of the car. But what car shape should be drawn?

E. F. Thacher, *A Solar Car Primer,* DOI 10.1007/978-3-319-17494-5_9

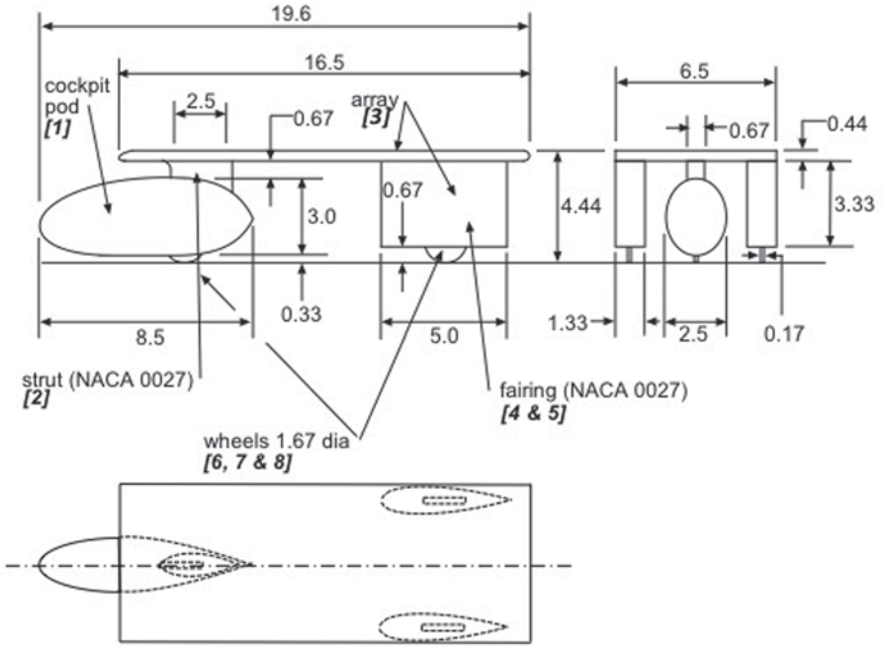

Fig. 9.1 Proposed solar racer (dimensions in feet)

9.3 The Table Top

The study of other solar racers that underlies the specification showed the great variety of solar racer shapes and provided starting ideas. Some cars emphasize solar collection and are essentially rolling tabletops. Others emphasize low drag and so have the solar array integrated into their streamlined body. However, even though the top cars are often streamliners, suppose the ideas uppermost in thought are that solar collection must be maximized and that the extra drag that this may cause could be compensated for by large wheel fairings which could supply thrust in cross-winds. Suppose research has shown that the prevailing winds blow across the race route; hence, the design's "secret weapon" will be the ability of the car to sail.

Figure 9.1 shows a drawing done from a freehand sketch of a three-wheeled[1] solar racer with a flat solar array on top, large rear sailing fairings, and a streamlined cockpit pod located in front. We will call it the "Table Top." Using only three wheels reduces the weight. The tricycle wheel arrangement allows the front structure of the car to be simplified with the front wheel housed in the cockpit pod. To provide sufficient room for the rear wheels and low drag, the cross-section profiles of the rear fairings and the pylon supporting the front of the solar array are symmetric, 27%-thickness-ratio airfoils with the maximum thickness at 30% of the chord from the leading edge. The car complies with Chap. 16, Sect. 16.1.1.1.

[1] Three-wheeled cars were not allowed in the 1999 Sunrayce.

9.4 Table Top Drag Estimate

The concept sketch will now be used to estimate the as-built drag area. If the drag area is satisfactory, the weight and other characteristics will be estimated.

We will make the estimate at 40 mph (17.88 m/s). A quarter-scale model of this vehicle was tested in a wind tunnel[2] at the Reynolds number corresponding to 40 mph (160 mph tunnel wind speed) and an atmospheric pressure and temperature of 99.6 kPa and 23.3 °C, respectively. We will estimate the drag coefficient for these conditions so we can compare it with the tunnel measurements.

Experience has shown that the drag area of the actual vehicle will usually be larger than that found by calculation, even those done using sophisticated computer programs.[3] This is caused by the many features, small and large, that computer models may overlook: seams between parts of the car, surface finish, the edges of solar cells, finite-radius trailing edges, the scooping of air into wheel fairings, etc. Therefore, the actual, as-built, drag area of the car must be measured. This may be done by full-scale wind tunnel, coast-down, or constant-speed testing.

Full-scale wind tunnel services are very expensive, and large wind tunnels are not usually nearby, nor accessible to solar car teams. Smaller wind tunnels for testing scale models are more accessible, and testing time in them is less expensive than that of full-scale tunnels. Scale-model testing can come closer to the as-built drag area because some of the features missed by simulations can, if properly scaled, be included.

Method As described in Chap. 17, the *drag build-up* method estimates the drag area and drag coefficient by modeling the car as a composite of shape elements which have known drag coefficients. The drag areas of these shape elements are corrected (as appropriate) for interference, ground effect, and roughness, and added to give the drag area of the car at a particular speed.

We study the Table Top and divide it up into eight component shapes. The profile areas of these shapes are designated A_1–A_8 in Fig. 9.1 (bracketed numbers in italics). The corresponding drag forces are D_1–D_8. Equation (17.2) is then applied to each shape.

At the wind tunnel ambient conditions Eq. (2.3) gives

$$\rho = \frac{p}{RT} = \frac{99.6\text{kPa}}{0.287\dfrac{\text{kJ}}{\text{kg}\cdot\text{K}} \times 296.45\text{K}} = 1.17\frac{\text{kg}}{\text{m}^3}$$

as the air density. The Reynolds number per unit characteristic length will be handy. The letter "L" symbolizes any characteristic length.

$$\frac{R_e}{L} = \frac{\rho V}{\mu} = \frac{1.17\dfrac{\text{kg}}{\text{m}^3} \times 17.89\dfrac{\text{m}}{\text{s}}}{18.39(10^{-6})\dfrac{\text{kg}}{\text{m}\cdot\text{s}}} = 1.14(10^6)\text{m}^{-1}$$

[2] See Chap. 12.

[3] Kurtz (1980) suggests on the order of 20 % higher.

The free-air dynamic pressure is

$$q = \frac{1}{2}\rho V^2 = \frac{1}{2} \times 1.17 \frac{\text{kg}}{\text{m}^3} \times \left(17.89 \frac{\text{m}}{\text{s}}\right)^2 = 189.23\text{Pa}.$$

Pod, A_1 The pod has an elliptical cross-section and is somewhat more elongated at the downstream end. We select an ellipsoid as the shape most closely approximating the pod, and for which data are available.

1. ***Free Air:*** The profile area of the pod, A_1, is

$$A_1 = \frac{\pi ab}{4} = \frac{\pi \times 3\text{ft} \times 2.5\text{ft}}{4} = 5.89\text{f}^2 = 0.547\text{m}^2.$$

The drawing shows the length of the pod as 8.5 ft, or 2.59 m. This is the characteristic length. The Reynolds number is

$$R_{\text{eL}} = 1.14(10^6)\text{m}^{-1} \times 2.59\text{m} = 2.96(10^6)$$

This implies turbulent flow, as Fig. 2.6 shows. The ellipsoid data of Table 17.1 are for a circular cross-section. Therefore, we calculate the pod's fineness ratio (length over diameter) as 3.1, using the diameter of the circle having an area equal to A_1, 2.74 ft. This technique was used by Kurtz (1980) when characterizing the fineness ratios of passenger cars. The turbulent flow column of Table 17.1 gives an estimate for $c_{\text{D}\infty}$ of 0.11.

2. ***Ground Effect:*** From Fig. 9.1, the minimum clearance ratio is about 0.13. The pitch angle is zero. The zero-pitch-, zero-camber-ratio teardrop in Chap. 17 is the closest to the ellipsoid shape. Using Eq. (17.17) and the zero-camber-ratio constants from Table 17.6 gives

$$\frac{\Delta c_{\text{DG}}}{c_{\text{D}\infty}} = -0.1256 + 0.1541\left(\frac{0.33\text{m}}{2.5\text{m}}\right)^{-1} - 0.0041\left(\frac{0.33\text{m}}{2.5\text{m}}\right)^{-2} = 0.807.$$

Figure 17.10 shows $c_{\text{D}\infty} = 0.078$. Hence,

$$\Delta c_{\text{DG}} = 0.078 \times 0.807 = 0.063.$$

3. ***Interference:*** There is interference between the pod and the strut and the front wheel. The extra drag is apportioned between the pod, the strut, and the wheel. We cannot estimate how much is apportioned to each. So, we will place all the interference drag on the strut or the wheel. Hence, for the pod: $\Delta c_{\text{DI}} = 0$.
4. ***Roughness:*** .For the smooth-skinned model, there is no extra roughness, so $\Delta c_{\text{DR}} = 0$.
5. ***Protuberances:*** There are no protuberances, such as rear view mirrors or antennae: $\Delta c_{\text{DP}} = 0$.

Strut, A_2 The strut has a NACA 0027 cross-sectional shape.

1. ***Free Air:*** Figure 9.1 shows the chord length as 2.5 ft and the thickness and average span as 0.67 ft. This chord gives a Reynolds number of $8.7(10^5)$. Tables 17.2 and 17.3 give drag coefficients, based on the planform area (chord × span), of several NACA airfoils at zero angle of attack. These data apply to wings of infinite span having the listed profile over the entire span. However, we take these to be an adequate approximation and note that the drag coefficient increases approximately linearly with the thickness ratio, but at the higher thickness ratios it decreases with Reynolds number. Using these observations to extrapolate gives a drag coefficient of 0.0092 at $Re_C = 1.75(10^6)$ for the NACA 0027. Finally, using the NACA 0025 Reynolds number dependence, because its thickness ratio is closest to 27%, we estimate a drag coefficient of 0.0096 at the operating free-air Reynolds number for the NACA 0027. The drag on the airfoil must be the same irrespective of the reference area. Therefore, we correct this planform-referenced drag coefficient to a profile-area-referenced value by dividing by the fractional thickness ratio.

$$c_{D\infty} = (c_{D\infty})_{\text{planform}} \frac{A_{\text{planform}}}{A_{\text{profile}}} = (c_{D\infty})_{\text{planform}} \frac{c \times \text{span}}{t \times \text{span}} = \frac{0.0096\text{m}}{0.27\text{m}} = 0.036$$

2. ***Ground Effect:*** The strut is shielded from the ground by the pod: $\Delta c_{DG} = 0$.
3. ***Interference:*** The strut causes interference drag at each surface to which it is attached. Equation (17.12) gives the interference drag for a strut with a wall at one end for t/c a little higher than 27%. An adequate estimate may be obtained by multiplying this equation by two. We use Eq. (17.14) to reference Δc_{DI} to the profile area, A_2.

$$\Delta c_{DI} = \frac{\Delta D_I}{qA_2} \approx 2[0.8(.27)^3 - 0.0003]\frac{(0.762\text{m})^2}{(0.204\text{m})^2} = 0.43$$

The interference drag is large. It can be reduced by using fillets at each end of the strut and reducing t/c considerably. This raises a question of strength. However, let us complete the estimate for the entire car first.

4. ***Roughness and Protuberances:*** We neglect these two effects as we did for the pod.

Solar Array, A_3 The drag of this component will be estimated for a smooth surface (no solar cells) so a comparison with wind tunnel data on the model car can be made. There are no shape element data for the array as a whole. Total drag could be estimated as the sum of friction drag and pressure drag from trailing edge separation: $D_3 = D_{3f} + D_{3P}$. However, the nose of the array is rounded, its trailing edge is tapered, and it has a large length-to-thickness ratio (greater than 37). Therefore, since the friction is proportional to the surface area, and the pressure drag depends approximately only on the shape of the leading and trailing edge, we assume $D_{3P}/D_{3F} << 1$,that is, the pressure drag force will be negligible compared to the friction drag.

1. ***Free Air:*** Figure 9.1 shows the length as 16.5 ft (5.03 m), width as 6.5 ft (1.98 m), and the thickness as 0.44 ft (0.134 m). Using the length gives a Reynolds number at the trailing edge of $5.73(10^6)$. This means that the flow is turbulent when it leaves the trailing edge.[4] We assume that the laminar–turbulent transition takes place at a Reynolds number of $3(10^6)$, that is, the plate is very smooth. Using this "critical" Reynolds number gives the distance from the leading edge to the transition as 2.63 m. Equation (17.20) gives the friction drag coefficient.

$$c_{DF} = \frac{1.328}{(3\times10^6)^{1/2}}\frac{2.63\text{m}}{5.03\text{m}} + \frac{0.031}{(5.73\times10^6)^{1/7}}\left[1-\left(\frac{2.63\text{m}}{5.03\text{m}}\right)^{7/8}\right] = 0.00185$$

This must be turned into a drag coefficient referenced to the profile area of the array. We assume that c_{DF} is uniform over the entire surface. The area of the array, including the sides but less the area of its underside taken up by the strut and the two fairings, is 20.74 m^2. The drag force is then

$$D_{F3} = c_{F3}A_{S3}q = 0.00185\times20.74\text{m}^2\times187.23\frac{\text{N}}{\text{m}^2} = 7.18\text{N}.$$

The profile area of the array is 0.266 m^2. The friction drag coefficient, referenced to the profile area of the array, is therefore

$$c_{D3} = \frac{7.18\text{N}}{0.266\text{m}^2\times187.23\frac{\text{N}}{\text{m}^2}} = 0.144.$$

This will be $c_{D\infty}$ for the arra.

2. ***Ground Effect:*** None (reasoning as for the strut).
3. ***Interference:*** Interference is present, but we will continue to add it to the other shape elements that attach to the array.
4. ***Roughness and Protuberances:*** None (as explained).

9.5 Fairings A_4 and A_5

1. ***Free Air:*** Proceeding as for the strut, we get a free-air-drag coefficient of 0.036 for each fairing.
2. ***Ground Effect:*** Assume that the effect of proximity to the ground is not large since most of the area of the fairing is at a large clearance ratio. This correction will then be zero.
3. ***Interference:*** The junction of each fairing with the solar array causes interference drag, as does the proximity of the fairings to each other.

[4] Critical Reynolds number $5(10^5)$–$3(10^6)$, with upper limit for a very smooth plate.

In the first case, notice that Fig. 9.1 shows that the outer surface of each fairing is approximately even with the outer edge of the array. We judge that this arrangement reduces the total interference drag from the two fairings to that for one alone. Using the "one end" wall interference correction as $\Delta c_{DI} = 0.087$, or 0.0435 per fairing.

Figure 17.5 shows the mutual interference between two airfoils in parallel. The ratio of the minimum spacing to the airfoil thickness is 2.887. From the free-air-drag coefficient in Fig. 17.4 and Eq. (17.8) we get for each of the pair of foils:

$$\Delta c_{DI} = 0.199 \times 0.0662 = 0.0132.$$

The total interference on each fairing is $\Delta c_{DI} = 0.0562$.

4. ***Roughness and Protuberances:*** None.

9.6 Wheels, A_6, A_7, and A_8

The wheel wells of the model were filled, and the wheels themselves were simply fixed, partial discs with small profile areas. Also, when tested in the wind tunnel, these disks were suspended a small distance above the tunnel's ground plane. We nevertheless treat them as real, stationary wheels in contact with the ground. Figure 9.1 gives the wheel diameter of 1.67 ft (0.508 m), the wheel width as 0.17 ft(0.052 m), and the projected un-faired height, 0.33 ft(0.1 m) and 0.67 ft(0.2 m) for the front and rear wheels, respectively. We take the c_D of an isolated, stationary wheel in contact with the ground to be 0.526 (Fig. 17.3). Following the wheel drag discussion in Chap. 17, we take the drag coefficient of the exposed portion of the shielded wheel (a wheel in a fairing or wheel well) to be approximately the same as the unshielded wheel. The drag area of a shielded wheel is therefore equal to the profile area of the unshielded part of the wheel times 0.526.

We ignore interference between the pod and the front wheel because the wheel is small compared to the pod.

9.7 Results

Table 9.1 summarizes the results. Note that the projected areas, $A_{D\#}$, may be summed to give A_D because all of each $A_{D\#}$ appears in the front view.

The estimated c_D of the car is therefore 0.141.

Discussion The Table Top's drag coefficient was measured at 0.139 in a wind tunnel at the National Research Council of Canada's Advanced Aeronautical Laboratory under the conditions mentioned at the beginning of the preceding calculation.[5] The calculation overestimated the drag coefficient by 1.4%.

[5] Chapter 12 "Testing," describes the construction of the quarter-scale model of the Table Top and presents some of the data from the tests.

Table 9.1 Table top drag area

#	$A_{D\#}$	$c_{D\infty}$	Δc_{DG}	Δc_{DI}	c_D	$c_D A_D$
1	0.547	0.110	0.064	0	0.174	0.0952
2	0.042	0.036	0	0.43	0.466	0.0200
3	0.266	0.141	0	0	0.141	0.0383
4	0.412	0.036	0	0.056	0.092	0.0380
5	0.412	0.036	0	0.056	0.092	0.0380
6	0.0063	–	0	0	0.526	0.0033
7	0.0063	–	0	0	0.526	0.0033
8	0.0052	–	0	0	0.526	0.0029
$A_D = 1.697 m^2$				$c_D A_D = 0.2390 m^2$		

The results are within an expected error of about 10%. Changes in some of the assumptions could certainly alter the results by several percent. Recall the earlier remark that because construction adds flaws and unavoidable features not included in the calculation, such as seams between body panels, the drag coefficient of the as-built, full-scale car will be higher still, and therefore also its drag area. And note that the drag area is greater than the specified limit of 0.11 m^2 (specification 8.5.1). The Table Top concept is rejected because its predicted drag area will be irredeemably greater than the limit specified.

9.8 The Shark

Another shape concept must now be considered. Morelli (1983) reported extensive tests of basic body shapes designed to have low drag near the ground. Some configurations of these shapes had extraordinarily low drag coefficients, around 0.05. And these figures were from tests, not calculations, albeit for smoothed, basic shapes. But beginning with such a low drag shape would provide a large margin between the specified drag area and the basic shape drag area to allow for the drag increase caused by transforming a smoothed model into a real car. However, the sloping, compound-curved Morelli shape would reduce the power of the solar cell array compared to one installed on the Table Top.

Figure 9.2 is a hand-drawn sketch of the Morelli shape concept, which we will call the "Shark," showing its principal features. A cross marks the estimated CG for each mass. No internal structural members are shown, other than the roll frame, a substitute for the rule-described roll bar, against which the driver reclines. The crosshatched paper enables projected areas to be estimated by counting squares.

The wheels are enclosed in fairings for streamlining and sailing and are arranged in a two in front–one in rear (2F-1R) wheel configuration. A three-wheel configuration will be lighter than a four-wheel one. The 2F-1R configuration is more stable

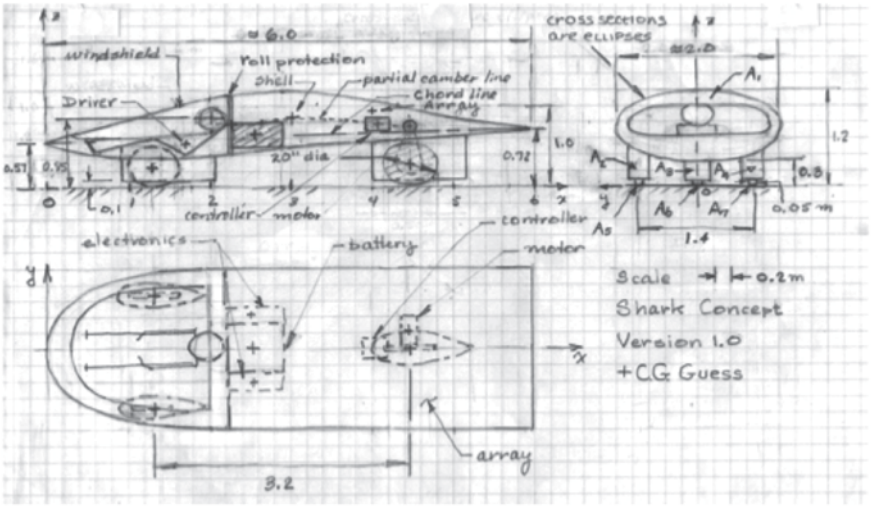

Fig. 9.2 Shark concept (dimensions in meters)

when turning and braking, which is the most common emergency maneuver.[6] A means for the fairings to accommodate large steering angles must be developed. The driver is in a near-reclining position. Achieving the view angles from the cockpit required by the race rules looks problematical. However, the low-drag potential of the shape is enormously attractive, and so we will continue to develop the concept. The shape has been drawn with a slight pitch-down attitude. This may slightly increase the drag above that for zero pitch. However, it may give a more negative lift coefficient, which may be a safer condition. Also, the drag of the ventilation system, array, or rear view mirrors will not be estimated at this stage.

9.9 Shark Drag Estimate

Let $p_\infty = 101.3$ kPa and $T_\infty = 25^\circ$C, then $\rho_\infty = 1.18$ kg/m^3. The drag will be evaluated for straight-ahead flow, 55 mph, or 24.58 m/s, and no wind. The Reynolds number per unit characteristic length and the dynamic pressure are

$$\frac{R_e}{\lambda} = \frac{1.18\dfrac{\text{kg}}{\text{m}^3} \times 24.58\dfrac{\text{m}}{\text{s}}}{18.46(10^{-6})\dfrac{\text{N}\cdot\text{s}}{\text{m}}} = 1.57(10^6)\text{m}^{-1},$$

$$q = \frac{1}{2} \times 1.18 \times (24.58)^2 = 356.5\frac{\text{N}}{\text{m}^2}.$$

[6] See Chap. 21.

Body, A_1 Counting squares in Fig. 9.2 gives A_1, the profile area of the basic shape, as about 1.45 m^2. The pitch angle, α, the angle between the chord line and the horizontal is about -1.43°. Since the body's length is 6.0 m, the chord, c, is slightly longer, but still about 6.0 m. A low camber ratio[7] is best because it provides a flatter surface for the array while still giving low drag. The maximum camber is about 0.22 m. Thus, the camber ratio is 3.67%. The lowest camber ratio reported by Morelli (1983) was 3.7%.

The clearance ratio is about 0.15. The design Reynolds number, chord times Re/λ, is 9.4(10^6), twice the value at which the Morelli data were taken. Therefore, the c_D will be somewhat underestimated because it trends upward as Re increases past the transition to turbulence. (See the ellipse curve in Fig. 2.6, for example.)

1. ***Free Air:*** Figure 17.8 gives $c_{D\infty} = 0.045$ for 3.7% camber ratio and $\alpha = 0°$. Since the pitch is outside the $\pm 1°$ range, this will be rounded up to 0.05.
2. ***Ground Effect:*** Equation (17.16) with the 3.7% camber ratio data of Table 17.5 gives $\Delta c_{DG}/c_{D\infty} = 0.1$; hence,

$$\Delta c_{DG} = 0.1 \times 0.05 = 0.005.$$

9.10 Front Fairings, A_2 and A_4

1. ***Free Air:*** The chord is 1.15 m with a maximum thickness of 0.24 m. The thickness ratio is therefore 0.21. The average span is about 0.35 m. The profile shapes approximate trapezoids. Thus, the product of the thickness and the average span gives the profile area, A_2 or A_4, as 0.084 m^2. Using Re/λ and the chord as the characteristics length, the Reynolds number at the fairing is 1.81(10^6). Extrapolating in Table 17.2 using NACA 2421 gives $c_{D\infty} = 0.0081$ based on the planform area, and dividing by t/c, 0.21, gives $c_{D\infty} = 0.039$ referenced to the profile area.
2. ***Interference:*** The interference drag between each fairing and the underbody of the basic shape and the mutual interference between the front fairings will be found in the same way as for the rear fairings of the Table Top.

From the sketch of the Shark, the minimum spacing between A_2 and A_4, y_{MIN}, is about 1.15 m. Hence, $y_{MIN}/t = 1.15/0.24 = 4.79$. For this dimensionless spacing, Figure 17.4 shows a nearly zero mutual interference drag between A_2 and A_4. For the interference between A_2 or A_4 and the underbody, Eq. (17.12) gives

$$\Delta c_{DI} = [0.8(0.21)^3 - 0.0003]\frac{(1.15\text{m})^2}{0.24\text{m} \times 0.35\text{m}} = 0.11.$$

3. ***Roughness, etc.*** None, as before.

[7] Camber ratio (%) is (maximum camber/chord) × 100; see Chap. 17.

Table 9.2 Initial Shark drag area

Piece #	$A_{D\#}$	A_P	$c_{D\infty}$	Δc_{DCG}	Δc_{DI}	c_D	$c_D A_{D\infty}$
1	1.500	1.500	0.05	0.005	0	0.055	0.0828
2	0.085	0.085	0.039	0	0.110	0.149	0.0126
3	0.080	0.154	0.033	0	0.146	0.179	0.0275
4	0.085	0.085	0.039	0	0.110	0.149	0.0126
5	0.005	0.005	0.526	0	0	0.526	0.0026
6	0.005	0.005	0.526	0	0	0.526	0.0026
7	0.005	0.005	0.526	0	0	0.526	0.0026
A_D	1.763					$c_D A_D$	0.1430

Rear Fairing, A_3 The rear fairing also has a chord of 1.15 m. It was given a thickness of 0.32 m because it may house the rear brake disk and caliper and portions of the drive (and possibly a wheel motor). It has a thickness ratio of 0.28 and a profile area of 0.154 m^2. We assume that the front fairings do not significantly affect the flow around A_3. Thus, the same chord Reynolds number calculated for the front fairings will be used for A_3. Extrapolating for NACA 0028 at a chord Reynolds number of 2.94(10^6) in Table 17.3 gives $c_{D\infty}=0.033$. Equation (17.12) gives $\Delta c_{DI}=0.146$. We make neither roughness nor protuberance corrections.

Wheels, A_5–A_7 We treat these in the same fashion as those of the Table Top. This gives a c_D of 0.526 per wheel.

Drag Area Table 9.2 summarizes the Shark results. The free-air profile areas, A_P, are in the third column. These do not necessarily sum to the front-projected area of the car.

The total drag area of 0.143 m^2 (rounded up) exceeds the specified drag area of 0.11 m^2, with the ventilation drag, array drag, and incidental drags from roughness introduced during manufacture still to be added.

Revision to Concept We will reduce the t/c ratio of the rear fairing, bearing in mind the drive elements it may contain besides the wheel. Fortunately, a relatively small reduction in thickness pays big dividends because the interference drag is a function of the thickness ratio cubed. Reducing t to 0.25 m gives t/c of 0.217 and a front-view profile area of 0.0625 m^2. The free-air profile area drops from 0.154 to 0.120 m^2.

The reduced thickness increases $c_{D\infty}$ to 0.037 but decreases the interference drag coefficient of the fairing from 0.146 to 0.087. The free-air profile area of the fairing shrinks to 0.120 m^2 and the front-view profile area from 0.080 to 0.0625 m^2. The latter reduction shrinks the profile area of the car to 1.746 m^2. The total drag area drops from 0.143 to 0.128 m^2.

Fillets extending downstream from the maximum thickness location of each fairing cause additional reduction in drag area. The fillet radius should be 4–8 % of the chord of each fairing (0.046–0.092 m in this case) and the length of the fillet downstream of the fairing trailing edge equal to the chord (Hoerner 1965). This trailing length and radius choice can reduce the interference drag to 1/10 (or less), of its no-fillet value, at a t/c of 0.2–0.25.

Recalculating the drag area for the car with the fairing interference drag at 1/10 of its no-fillet value gives 0.104 m^2. This range leaves about a 5.5 % margin for the other sources of drag not included in the current estimate. Also, after considering the wheel and suspension design, we may find that the profile areas of the fairings can be reduced further, thus increasing this margin. Figures 9.10 and 9.11 show the car with the fairing fillets added.

The aerodynamics are marginally satisfactory, so far. We pass to consideration of the weight and CG.

9.11 Shark Weight and CG

Weight Control "Weight control" means not just how much weight but the distribution of weight. The weight and its distribution is much easier to control if the car is finished early in an orderly way, say by the summer or fall preceding the race (American Solar Challenge schedule). It is more difficult to control if the car is built at the last minute, that is, during the spring before the race. Control requires a procedure to track the weight of the car and to allot weights to different systems; and a firm resolve[8] to stick to the procedure, specification, and allotment.

Results The mass of the vehicle must satisfy specification 8.4 and the CG location must satisfy specification 8.11.1.

The method of Chap. 21 was employed to estimate these parameters. The shell was assumed to be made of a Kevlar®–Nomex® composite sandwich having a density of 185.3 kg/m^3 (see Table 9.5). The masses of some of the components in Fig. 9.2 can be estimated from previous experience or manufacturer's data. The driver's mass is known to be 80 kg because the driver will be ballasted to that mass.

To make the estimate more realistic, set the construction of the internal stiffening structure of the car as shown in Fig. 9.3. The stiffener masses will be estimated based on carbon–foam composite construction. The plate-like shapes were assumed to have a uniform composition through their thickness and therefore that the CG is on the center plane of the plate. Hence, we calculate only the x, z or y, z coordinates of the CG, as appropriate. The left and right cage walls have a nonuniform construction, so they must be broken down into pieces. Table 9.3 shows the results for the stiffeners and the shell. Coordinate x is measured from the car's nose. Once the stiffeners' CG locations and masses are known, the structures may be treated as isolated masses, like the driver or the battery. Table 9.4 summarizes the guesses and estimates for the other components.

The calculation gives the vehicle's gross mass as 320.2 kg, with the CG located at an x-coordinate of 2.618 m, a y-coordinate of 0.008 m, and a z-coordinate of 0.641 m. The off-centerline CG location is caused by the off-centerline location of

[8] That is, management must be really hard-nosed about it.

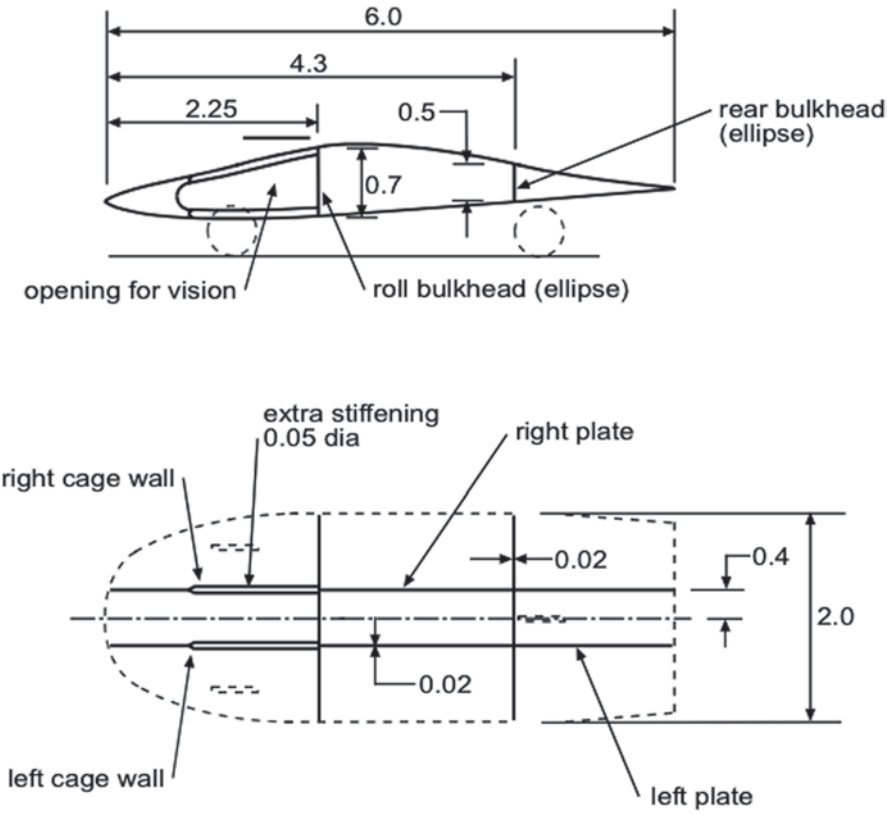

Fig. 9.3 Tentative internal structure (dimensions in meters)

Table 9.3 Stiffener and shell CG coordinates

Stiffener	x(m)	y(m)	z(m)	M(kg)
Left	3.5	0.4	0.85	2.0
Right	3.5	−0.4	0.85	2.0
Rear	4.3	0	0.8	2.0
Roll	2.25	0	0.8	2.5
Left cage	1.0	0.4	0.6	1.0
Right cage	1.0	−0.4	0.6	1.0
Shell	3.05	0	0.85	38.6

Table 9.4 Mass summary

Category	Mass (kg)
Wheels	5.19
Driver	80.00
Battery	140.00
Motor and Controller	24.60
Array and MPPTs	15.30
Shell	38.60
Fairings	6.00
Frame	10.50
SUBTOTAL (kg)	320.20
ALLOWANCE (kg)	17.80
Specification 4.3 (kg)	338.00

MPPT *maximum power point tracking*

Table 9.5 Shell moment of inertia

Seg.	I_{CG}(kg · m^2)	x_j(m)	x_jM_j(m · kg)	M_j(kg)	h^2(m^2)	I_{Zj}(kg · m^2)
1	1.146	0.50	2.330	4.660	4.554	22.370
2	1.146	1.50	10.525	7.017	1.286	12.090
3	3.293	2.50	18.234	7.294	0.018	3.427
4	3.064	3.50	24.558	7.017	0.750	8.329
5	2.606	4.50	29.079	6.462	3.482	25.109
6	2.125	5.50	32.339	5.880	8.214	50.425
Totals:			117.066	38.329		121.750

the CG of the motor; the other off-centerline CGs are balanced. Note that the *x*- and *z*-coordinates are close to the corresponding coordinates of the battery's CG.

The wheelbase is 3.2 m and begins 1.3 m from the nose, so the CG is spaced 41.1 % of the wheelbase from the front wheel contact patches, or 7.9 % outside of the specified zone of 33.3 % (specification 8.11.1). The steering, suspension, instruments, cabling, and lights were left out of the CG calculation. However, the battery and the driver are the strongest influences on the CG location.

The mass is 17.8 kg below the target, but, as noted above, a number of components were not included. The 17.8 kg is then an estimate of the mass allowance for these components (Table 9.3).

9.12 Rollover and Skid

Specification 8.11.5 governs here. Once the weight and CG calculations have been completed, sufficient information is known to estimate the rollover and skid stability. Use the traction limits of Chap. 21 ($a_x/g = 0.85$, $a_y/g = 0.75$), absent knowledge of the actual tires to be used by the Shark. Using the CG location, *L,* and *T* with

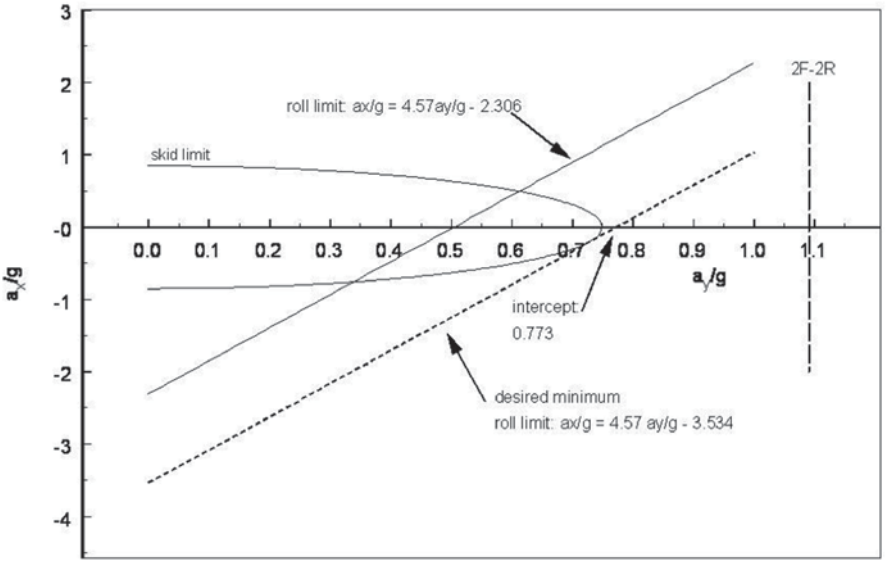

Fig. 9.4 Initial roll and skid limits

Eq. (21.32), the limiting rollover line has been plotted in Fig. 9.4. The prohibited operating regions are points to the right of the line.

The positive ordinate is the braking inertial force in *g*'s. The negative ordinate is the acceleration inertial force in *g*'s. Both are tangent to the path of the car's CG. The abscissa is the centrifugal inertial acceleration perpendicular to the path of the CG.

The car fails the specification in that the roll limit line is well inside the skid ellipse for $0.34 \lesssim a_y/g \lesssim 0.61$. For transverse accelerations to the right of this line, the car will roll before skidding as long as the braking or longitudinal acceleration is less than the skid limit.

A more subtle point is that even when turning at steady speed at a *g*-load less than the roll limit, the car could initiate a roll if the driver accelerates. For example, at a transverse acceleration of 0.45 *g*, the car will roll if the driver accelerates at about 0.25 *g*. This can only happen, however, between 0.34 and 0.5 transverse *g*: Below 0.34 *g*, the 0.25 *g* acceleration has no effect; above 0.5 *g* the car has already begun to roll. The destabilizing effect occurs because the moment of the rearward inertial force component adds to the tipping moment of the transverse acceleration in the 2F-1R wheel configuration.

The opposite effect happens if rolling has begun and the brakes are applied. If rolling at slightly more than 0.5 *g*, a little braking, say 0.1 *g*, would stop the roll, assuming the braking can be at least this effective with the outside front tire not in contact with the road. The moment of the forward inertial force opposes the tipping moment of the transverse acceleration. This effect makes the 2F-1R car safer in emergency obstruction avoidance, if the brakes are applied first. Suppose a deer

enters the road and the driver first brakes at 0.6 g and then turns right at 0.5 g, the Shark will not roll.

Using Eqs. (21.34) and (21.35), the line labeled "minimum desired" rollover limit has also been plotted in Fig. 9.4. This line has a 0.773 g intercept with the a_y/g axis. The wheelbase and the track set the slope (2 L/T) of the limit lines. If these are fixed, then this intercept means that

$$\frac{b}{h} \geq 3.534$$

to meet specification 8.11.5. The distance $b = L - a$, or 1.887 m.

Hence, b/h is actually 2.944. This constraint will require some changes in the Shark concept, if three wheels are retained, just to get the smallest acceptable b/h, 3.534. For instance, if b/L were increased to 0.67 as required for directional stability, say by moving the batteries forward beyond the roll bulkhead, then h should be no more than 0.607 m. This is a reduction of 3.4 cm. This could be done. The car could be lowered, for example, although this would increase the drag somewhat.

Increasing T/L would steepen the roll limit line and move it to the right. Race rules limit the width of the car to 2 m, so there is not much room to increase T. The car could of course be shortened. Although making the car smaller (which should reduce the weight, an important advantage) and lower is certainly an option, completely exploring all the implications of this is a lengthy process. Let us examine a direct way of meeting the stability requirements.

Two in Front–Two in Rear (2F-2R) The slope of the rollover line can be made vertical, independent of the CG location, and moved to the right by shifting to four wheels, as Eq. (21.31) shows. For the present design:

$$\left[\frac{a_y}{g}\right]_{a_x=0} = \frac{T}{2h} = \frac{1.4\text{m}}{2 \times 0.641\text{m}} = 1.09g.$$

This rollover limit line is the vertical broken line in Fig. 9.4.

If we were to move to a four-wheeler, and assuming the CG height were about the same, the above intercept would be adequate. It would provide an allowance for the compliance of the suspension and the tires (neglected in Chap. 21), and for a transverse skid limit greater than 0.75 g. Notice also that b/L satisfies now-governing specification 11.8.3 because (if adding another wheel does not shift the CG much farther rearward) it is already less than 0.5. We would be out of the woods.

The downside of four wheels is somewhat increased weight, rolling resistance, drag, complexity, and cost. However, we may be able to compensate for the first three of these negative effects by reducing weight (perhaps by moving to a shell-and-space frame design) and drag elsewhere and in the tire design. The extra complexity and cost we will have to accept. The gain in safety overrides these considerations. Let us evaluate the 2F-2R design.

Drag Area Keeping the wheelbase the same, we place the two rear tires directly behind the front tires. The rear track will then be 1.4 m. The current rear wheel fairing design, NACA0028 will be retained.

There will be, as in front, negligible interference between the rear wheels. However, interference between the front and rear fairings on each side is now possible. Using a dimensionless spacing (see Fig. 17.5) of 2.70 in Eqs. (17.10) and (17.11) for a front and rear wheel pair on each side gives decrease of −0.042 for each one of the front wheels but a drag increase of 0.012 for each of the rear wheels. (Here, we have assumed that the fillets have no effect on the interference. This may not be conservative.)

Using the 1/10 rule to reduce the interference drag with the shell and then superimposing the interference corrections gives the total profile drag area of

$$c_D A_D = 0.106 \text{m}^2.$$

The drag area margin that existed in the 2F-1R configuration has been reduced to 3.6%. The drag area will probably exceed 0.11 m^2, as-built. Using the 2F-2R wheel arrangement reduces the profile area to 1.684 m^2 so that the car's drag coefficient is 0.062.

Mass and CG Adding another wheel and fairing increases the total mass to 323.6 kg, rounded up. This is still acceptable. We place the motor over on the left rear wheel. Accounting for the extra mass of the new wheel and fairing then gives $x_{CG} = 2.624$ m, $y_{CG} = -0.020$ m, and $z_{CG} = 0.639$ m. And $a/L = 0.414$, within the 2F-2R stability limit, as expected.

9.13 Side Gust

The rollover limit is specification 8.5.2, which sets $V_W = 50$ kph, and $V_X = 88$ kph. We will use the ambient temperature of 25°C and pressure of 101.3 kPa required by specification 8.3.2 and set the ratio of the gust slope width to the vehicle's length at 1. Figure 21.5 shows the gust scenario.

Method Equations (21.3) will be solved for the car's trajectory using the "little tap" method of Chap. 2. The force and moment used in these equations will be approximated for each new time by the method in Chap. 21. Finally, the accumulated distance moved in the global y-direction (transverse to the traffic lane) and the change in the heading of the car will be calculated for each time. All the information needed for the calculation is known except the cornering stiffness of the front and rear wheels and the moment of inertia of the car about its CG.

Cornering Stiffness Roland (1973) gives an empirical equation for the cornering force developed on a wheel contact patch at zero camber angle as

$$\frac{F_Y}{F_Z} = (1 - 4.88 \times 10^{-4} F_Z)(12.95\alpha + 436.37\alpha^3).$$

We will assume the constants, derived for a bicycle tested by Roland, are typical of the bicycle-type tires used on solar racing cars.

Multiplying by the vertical force, F_Z, and dividing by the slip angle, α, gives an equation for the cornering stiffness as a function of the slip angle. Taking the average of this expression up to a slip angle of 3° and using the current weight distribution (929.8 N/wheel, front, 656.5 N/wheel, rear) gives the average front (F) and rear (R) cornering force coefficients (see Eq. (21.1))

$$\bar{C}_{\alpha\mathrm{F}} = 114.5\frac{\mathrm{N}}{\mathrm{dgr}} \text{ and } \bar{C}_{\alpha\mathrm{R}} = 101.1\frac{\mathrm{N}}{\mathrm{dgr}}.$$

Therefore, the understeer gradient (Eq. (21.5)) is

$$K = \frac{W_\mathrm{F}}{\bar{C}_{\alpha\mathrm{F}}} - \frac{W_\mathrm{R}}{\bar{C}_{\alpha\mathrm{R}}} = \frac{929.8\mathrm{N}}{114.5\frac{\mathrm{N}}{\mathrm{dgr}}} - \frac{656.5\mathrm{N}}{101.1\frac{\mathrm{N}}{\mathrm{dgr}}} = 1.630\frac{\mathrm{dgr}}{\mathrm{g}}.$$

There is no critical speed because the understeer gradient is positive.

Moment of Inertia The moment of inertia, I_Z, about the CG, will be estimated using the method of Chap. 21. I_Z must be known to estimate the effect of a side gust. The estimate for the shell is shown below. The shell was assumed to be made of a Kevlar®-faced Nomex® composite with a density of 93 kg/m^3 and a thickness of 3/8 in. (0.00953 m).

The canopy, which is integral with the shell, was assumed to have about the same density. The shell was divided into six 1-m-long segments. The cross-sectional shape of each segment, an ellipse, was given the major and minor axes dimensions read from Fig. 9.2 at the center of the segment. Thus, the approximated shape would have a stepped appearance. Table 9.5 shows the resulting I_Z of the shell: 121.75 kg·m^2.

The second column gives the moment of inertia of the segment with respect to its own CG, I_{CG}. This is equal to the difference between the I_{CG} of the elliptic cylinder having the major and minor axes of the segment and that of the elliptic cylinder concentric with it but having its major and minor axes reduced by the segment's thickness. For segment 1, the mass of the outer cylinder is

$$M_{\mathrm{O1}} = (\rho\pi abL)_1 = \pi \times 185.24\frac{\mathrm{kg}}{\mathrm{m}^3} \times 0.7\mathrm{m} \times 0.15\mathrm{m} \times 1\mathrm{m} = 61.11\mathrm{kg},$$

where "a" and "b" represent half the major and minor axes, respectively. Subtracting the thickness from a and b and recalculating gives

$$M_{\mathrm{I1}} = 56.45\mathrm{kg} \text{ and } M_1 = (M_O - M_I)_1 = 4.66\mathrm{kg}.$$

I_{CG1} is then (using a standard formula)

$$I_{\mathrm{CG}_1} = \left(M\frac{L^2}{12}\right)_1 + \frac{1}{4}(M_\mathrm{O}a_\mathrm{O}^2 - M_\mathrm{I}a_\mathrm{O}^2)_1 = 1.146\mathrm{kg}\cdot\mathrm{m}^2.$$

The squared distance from the CG of the segment to the CG of the car is

$$h_1^2 = (x_1 - x_{CG})^2 + (y_1 - y_{CG})^2 = (0.5\text{m} - 2.634\text{m})^2 + [0 - (-0.02\text{m})]^2 = 4.554\text{m}^2.$$

The parallel axis theorem then gives I_{Z1} as

$$I_{Z1} = I_{CG} + h_1^2 M_1 = 1.146\text{kg}\cdot\text{m}^2 + 4.554\text{m}^2 \times 4.66\text{kg} = 22.37\text{kg}\cdot\text{m}^2.$$

Completing the calculation of I_Z by adding in the other parts of the car (j=2, 3,…6) gives $I_Z = 389.88\text{kg}\cdot\text{m}^2$. The radius of gyration of the vehicle's mass is

$$r_g = \sqrt{\frac{I_Z}{M}} = \sqrt{\frac{389.88\,\text{kg}\cdot\text{m}^2}{323.6\,\text{kg}}} = 1.097\text{ m}.$$

Shell CG At the end of the fourth column of Table 9.5 is the sum of the products of the segments and the distances of their CGs from the nose of the car. Dividing this sum by the total mass of the shell gives the coordinate of the shell's CG.

$$x_{CG} = \frac{117.066\,\text{m}\cdot\text{kg}}{38.33\,\text{kg}} = 3.045\text{m}$$

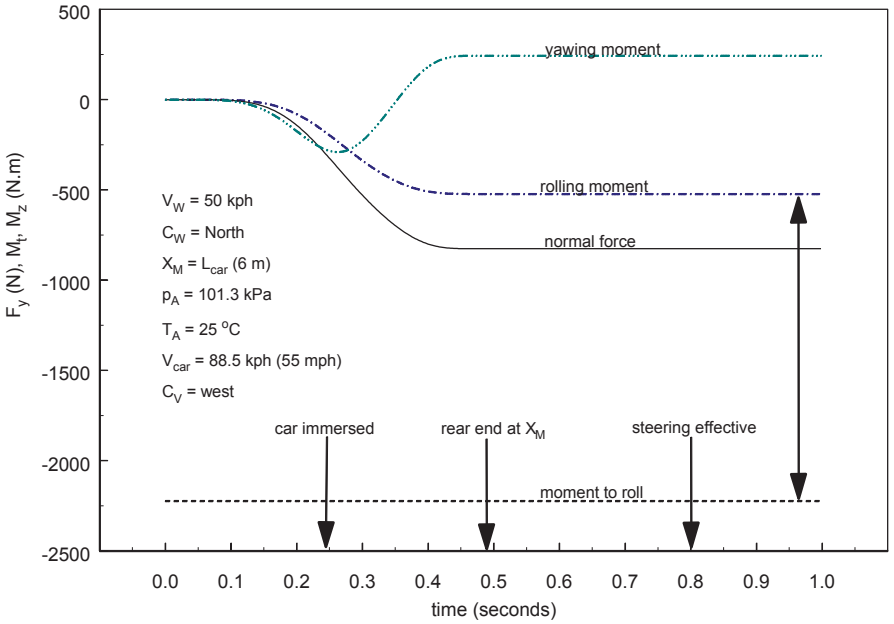

Fig. 9.5 Side force and moments on the Shark

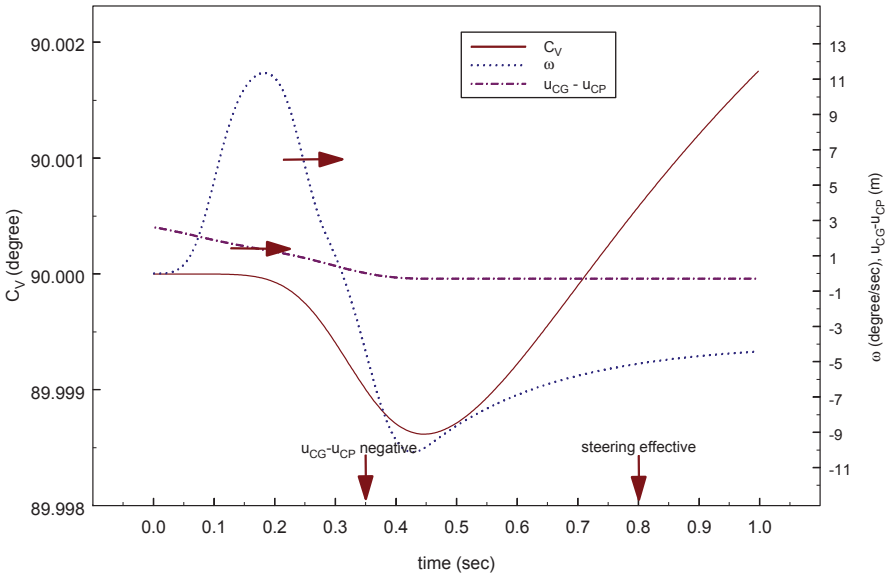

Fig. 9.6 Heading and heading velocity of the Shark

Results Figure 9.5 shows the side force, F_y, the yawing moment, M_z, and the rolling moment M_t. Also shown is the moment causing rollover, calculated as −2222.6 N m by Eq. (21.20). Note that, as the double-headed arrow indicates, there is a large clearance between the moment causing rollover and the maximum rolling moment.

The yawing moment is at first counterclockwise (less than zero) and then shifts to clockwise. This behavior is caused by the yawing moment arm,[9] a function of the car's shape, which is positive until about 0.35 s, then passes through zero and is negative thereafter. Hence, as Figs. 9.6 and 9.7 show, this causes the car to turn slightly north at first and then slightly south. The displacement of the car's CG in the traffic lane was minuscule, effectively zero, and therefore was not plotted.

The simulation results show that the car will be stable and will deviate only a negligible amount from a straight path under the design side gust conditions. However, the designer should bear in mind the limitations of the calculation. For example, Figure 9.7 shows that the car will not roll in a 100 kph gust. This is clearly not credible. Under such heavy aerodynamic loads, effects ignored in the model, used in the calculation will come into play. Lift is one such effect. A positive angle of attack to the relative wind would be produced by flexing of the suspension (also neglected in the model). This would cause upward lift and generate an additional aerodynamic rolling moment that would cause roll. The calculations presented here are intended as aids to design, not as revelators of absolute truth. They are not equivalents to wind tunnel testing of scale models. Nor should their results justify operating a solar car unwisely, such as in 100 kph wind gusts.

[9] The yaw moment arm, $u_{CG}-u_{CP}$, where u is the distance from the nose of the car and CP denotes the longitudinal coordinate of the center of pressure, is plotted in Fig. 9.6.

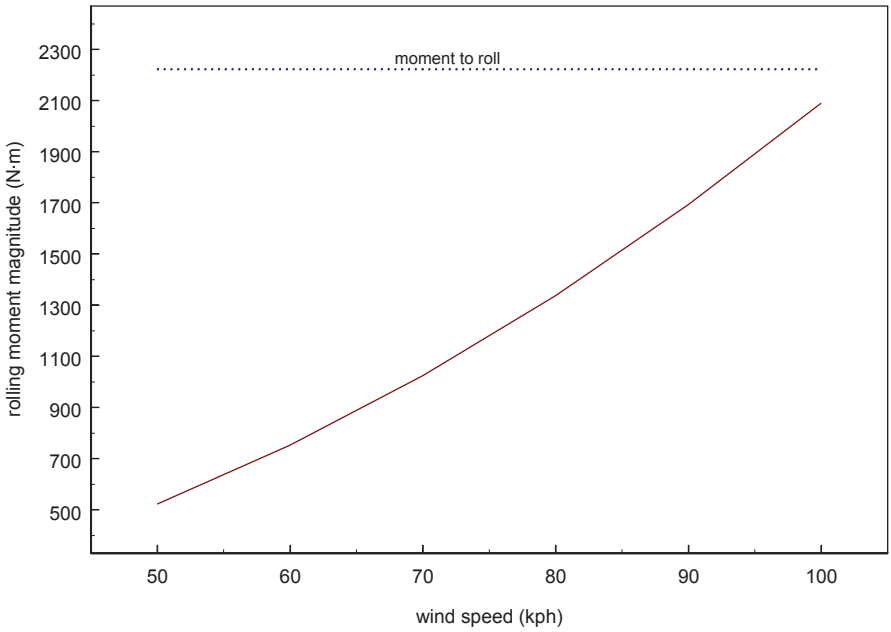

Fig. 9.7 Aerodynamic rolling moment study

9.14 Drive, Battery, Energy Rate and Range

Drive The design maximum grade and the design speed up this grade establish the maximum tractive torque and power required to climb hills. The design maximum grade should therefore not be less than the steepest grade in the design race route. The maximum cruising speed on a zero grade sets the maximum rotational speed.

The maximum grade in the design race route is 10% (specification 8.2.0). The speed up this grade is 40 kph. The maximum speed on a zero grade is 88.5 kph (55 mph). To allow for mass gain we will generate the requirements using the mass limit of 338 kg in specification 8.4.1. Multiplying the current maximum drag area estimate by an "as-built" factor of 1.2 gives a drag area 0.127 m^2. See Chap. 10, Table 10.2 for the drive procurement performance points.

Battery The details of the battery will be left to Chap. 10. However, in computing the weight of the vehicle, we have assumed that the battery's mass is 140 kg. Good-quality lead-acid batteries have a specific energy of about 35 W·h/kg. Using these batteries gives a total capacity of about 4900 W·h, of which about 80% (about 4000 W·h) is useable. Lead-acid batteries are the cheapest of the battery types allowed by the sample rules of Chap. 16.

Energy Rate and Range As an example, we will estimate the tractive energy consumption rate of the Shark using the drag areas estimated above and the conditions

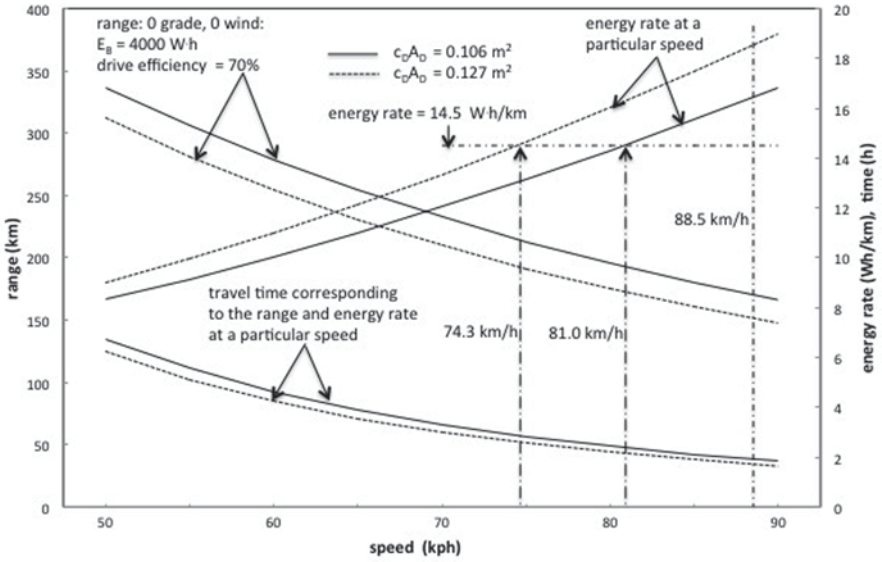

Fig. 9.8 Range and energy rate (battery only)

required by specification 8.13.1. This estimate will of course be revised several times during the design process as the information about the car becomes more complete and accurate.

Suppose the battery contains 4000 W·h of useable energy,[10] the efficiency, $\eta_{OVERALL}$, between the battery and the contact patch of the driven wheel is 70 %, and the rolling resistance coefficients are at the limits set in specifications 6.1 and 6.2. Let the mass be the maximum, 338 kg. Using these numbers, we will calculate the energy rate, range, and running time of the Shark on a horizontal road as a strictly battery-powered car. The energy rate, e_R, will be found from Eq. (2.17) and the range, *S,* from

$$S = \eta_{OVERALL} \frac{E_B}{e_R}.$$

Where E_B is the usable battery energy in W·h, and e_R is the energy rate in W·h/km.

The results are shown in Fig. 9.8. Notice that at the design speed the energy rate exceeds the specified value at both drag areas.[11] The car must cruise at 74.3 kph (46.2 mph) at the higher drag area and at 81 kph (50.1 mph) at the lower drag area to not exceed the design rate.

[10] This is assumed constant for convenience. The capacity of the battery is actually a function of the current discharge rate; see Fig. 4.5.

[11] Recall that specification 8.13.1 is a "wish."

Reducing the speed to about 50 kph (31 mph) will give an energy rate of about 9 W·h/km and a range of about 320 km (200 miles). Travel time would be 6.4 h.

9.15 Array Concept

In Fig. 9.2 we have already established the underlying shape and, by implication, the maximum area of the array. And, for the weight calculation, we assumed four parallel strings, each with its own maximum power point tracking (MPPT). Further array details will be left to the next chapter.

9.16 Driver Interface

Visibility The next step in the development will be to check the driver position for minimum height-of-eye and the side and forward view angles from that position (see Chap. 16, **Sect. 16.6.6**). The rear view system will be postponed to the next chapter. Figure 9.9 shows, except for the rear vision requirements, that the Shark concept is within the rules if the canopy encompasses the angles shown.

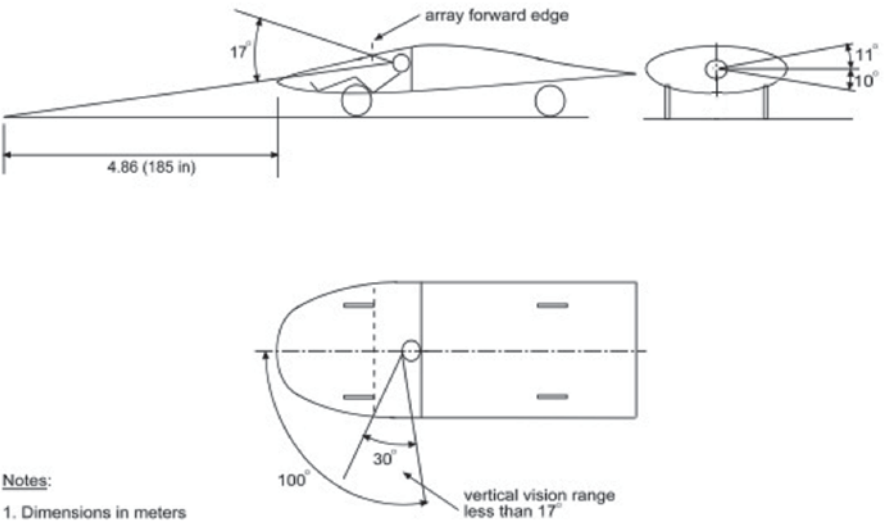

Fig. 9.9 Driver visibility study

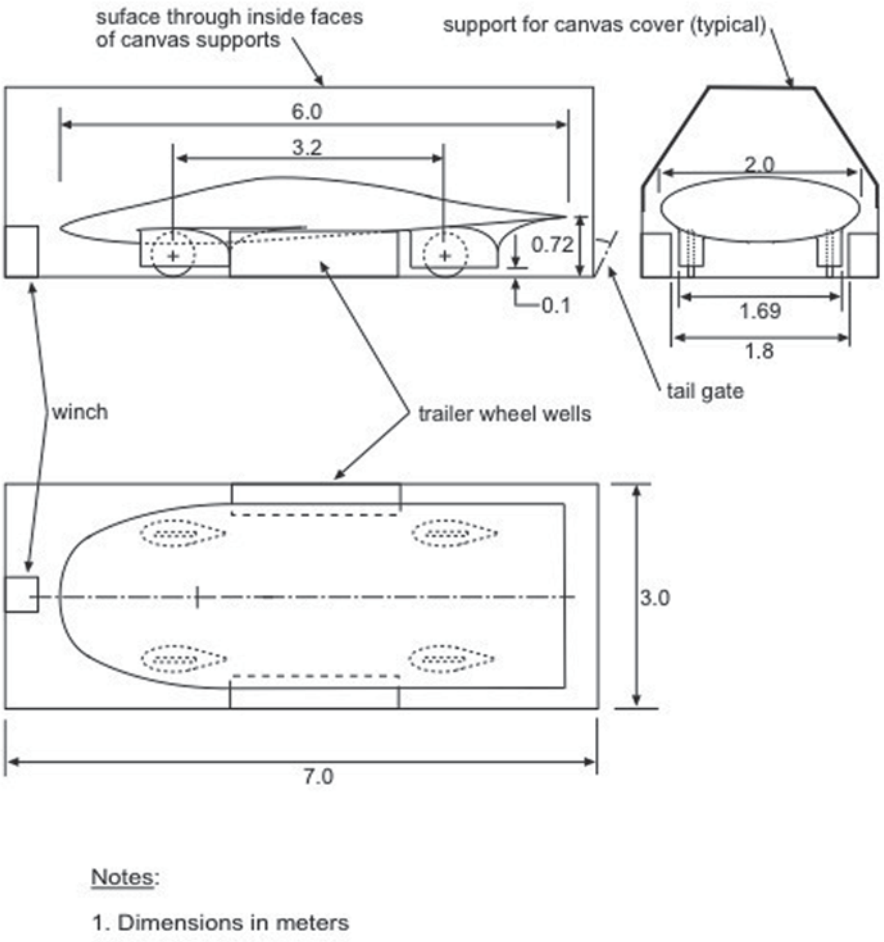

Fig. 9.10 Transport clearances

9.17 Transport Compatibility

Figure 9.10 shows the spacing between and the height of the wheel wells of an actual transport trailer. Comparison of these dimensions shows that the Shark will fit inside the trailer, although it is a close fit in some places. The vehicle will have to be carefully restrained and possibly padded in some places to prevent damage.

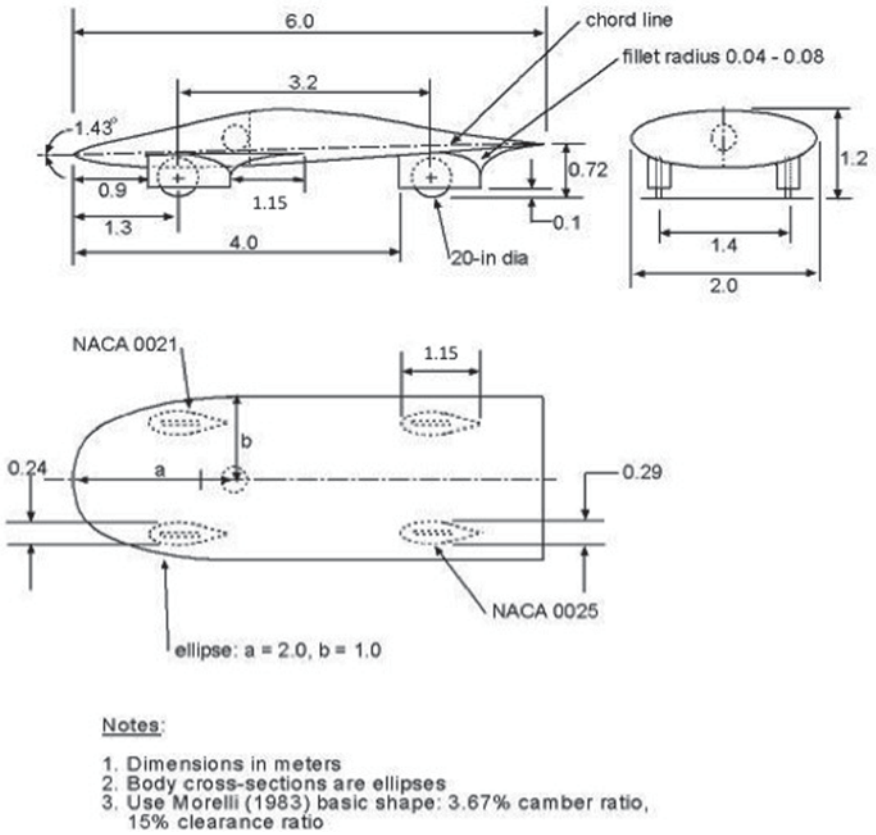

Fig. 9.11 Shark Layout

9.18 Concept Summary

Layout A three-view layout drawing is the end product of the conceptual design phase. Information for the drawing comes from the concept sketch and the calculations completed above. The drawing for the Shark is shown in Fig. 9.11. As Raymer (1989) points out, this drawing is the basis for further studies of the design and may be revised several times. Some way to accommodate the fairings to large steering angles must be devised.

Summary Table 9.6 summarizes the principal findings for the Shark, so far.

Table 9.6 Concept summary

Shape	Morelli "Shark": 3.7 % camber ratio, 15 % clearance ratio, −1.43° pitch angle.
Dimensions	Length = 6 m, max. height = 1.2 m, wheelbase = 3.2 m, track = 1.4 m, max. width = 2.0 m
Inertial	Mass = 323.6 kg, CG at $x = 2.624$ m, $y = -0.02$ m, $z = 0.639$ m
Aerodynamic	$c_D A_D = 0.106\ m^2 - 0.127\ m^2$, $A_D = 1.68\ m^2$
Array	Integral to Shark shape; four parallel strings each with an MPPT
Battery	Capacity ≈ 4000 W·h, efficiency ≈ 80 %
Drive	See study displayed in Fig. 9.8
Tractive energy rate	About 16.6–18.6 W·h/km at 88.5 km/h
Wheels	2F-2R, 20 in. outside diameter
Problems	1. Fairings at large steering angles 2. Rear vision from cockpit 3. Energy rate too high

MPPT *maximum power point tracking,* 2F-2R two in front–two in rear

References

Hoerner, S. F. (1965). *Fluid dynamic drag*. Bakersfield: Hoerner Fluid Dynamics.

Kurtz, D. W. (1980). Aerodynamic design of electric and hybrid vehicles: A guidebook. JPL Publication 80–69 (NASA-CR-163744 and NTIS N81–12943), Jet Propulsion Laboratory, Pasadena, California.

Raymer, D. P. (1989). *Aircraft design: A conceptual approach*. Washington, DC: American Institute of Aeronautics and Astronautics.

Roland, R. D. (1973). "Computer simulation of bicycle dynamics,". Mechanics and Sport, ASME Winter Annual Meeting, Detroit, Michigan, November 11–15, 1973, ASME, New York, pp. 35–83.